

## III-Nitride photon counting avalanche photodiodes

Ryan M<sup>c</sup>Clintock, Jose Luis Pau, Kathryn Minder, Can Bayram, and Manijeh Razeghi\*

Center for Quantum Devices; Department of Electrical Engineering and Computer Science;  
Northwestern University; Evanston, Illinois 60208; USA

### ABSTRACT

In order for solar and visible blind III-nitride based photodetectors to effectively compete with the detective performance of PMT there is a need to develop photodetectors that take advantage of low noise avalanche gain. Furthermore, in certain applications, it is desirable to obtain UV photon counting performance. In this paper, we review the characteristics of III-nitride visible-blind avalanche photodetectors (APDs), and present the state-of-the-art results on photon counting based on the Geiger mode operation of GaN APDs. The devices are fabricated on transparent AlN templates specifically for back-illumination in order to enhance hole-initiated multiplication. The spectral response and Geiger-mode photon counting performance are analyzed under low photon fluxes, with single photon detection capabilities being demonstrated in smaller devices. Other major technical issues associated with the realization of high-quality visible-blind APDs and Geiger mode APDs are also discussed in detail and solutions to the major problems are described where available. Finally, future prospects for improving upon the performance of these devices are outlined.

Keywords: Avalanche photodiodes, GaN, Photon counting, Photodetector, Ultraviolet

### 1. INTRODUCTION

Wide bandgap III-nitride semiconductors have been the subject of intense scientific and technological developments since the 1990's, primarily driven by the quest for blue lasers and high brightness visible light emitting diodes. In parallel, III-nitrides have also been studied extensively for use in ultraviolet (UV) photodetectors due to their potential to offer intrinsic visible- or solar-blind detection, which is highly desirable for a number of applications. Using a visible- or solar-blind detector dramatically relaxes the system requirements, eliminating the need for expensive and efficiency-limiting optical filters to remove undesired out-of-band photons. Thus, visible- and solar-blind UV photodetectors find uses in numerous applications in the defense, commercial, and scientific arenas. These include covert space-to-space communications, early missile threat detection, chemical and biological threat detection and spectroscopy, flame detection and monitoring, UV environmental monitoring, and UV astronomy.<sup>1,2,3</sup>

However, many of these applications are still dominated by the use of photomultiplier tube (PMT) based UV detectors. PMTs obtain high sensitivity by taking advantage of internal gain (typically  $\sim 10^6$ ), however these detectors are bulky, fragile glass tubes that require large biases (typically 1000 V) to operate effectively.<sup>4</sup> Therefore, it is highly desirable to have a smaller semiconductor-based photodetector capable of realizing this level of sensitivity.<sup>5</sup> In semiconductors it is possible to obtain internal gain by taking advantage of avalanche multiplication under high electric fields. Unlike photoconductive gain earlier reported in (Al)GaN based devices,<sup>6</sup> avalanche gain is in principle capable of providing lower noise and faster response times thus increasing the sensitivity of these photodetectors.

Great strides have been made in the realization of UV avalanche photodiodes<sup>7,8,9,10,11</sup> based on III-Nitrides. Most of the early GaN APD devices were designed for front-illumination operation with photons reaching the p-layer first. This configuration has been mostly used historically because one would get fewer defects by growing a device structure on several-micron thick n-type GaN templates on sapphire or even GaN substrates. However, there is a strong scientific and technological desire to investigate back-illuminated GaN avalanche photodiodes for a number of reasons. A back-illuminated p-i-n GaN structure, in which photons reach the n-layer first, allows the device to take advantage of hole initiated multiplication, since hole impact ionization coefficients are higher than the electron coefficient in GaN.<sup>12</sup> We have experimentally confirmed that hole-initiated multiplication provides superior

---

\* razeghi@eecs.northwestern.edu; phone 1 (847) 491-7251; fax 1 (847) 476-1817; <http://cq.d.eecs.northwestern.edu>

performance in linear mode GaN APDs due to the higher hole ionization coefficient;<sup>13</sup> back-illumination maximizes the injection of holes into the multiplication region making it a better approach in p-i-n avalanche photodiodes. In addition, the integration of APD arrays with read-out electronics becomes easier.

However, an APD alone is not sufficient for many of the applications listed above, and there is a need to develop single-photon detection capabilities in UV detectors. This is accomplished through the use of Geiger mode operation; this entails the operation of an avalanche photodiodes well above the breakdown voltage in combination with quenching circuitry. In Geiger mode the electric field is sufficiently high that a single charge carrier injected into the multiplication layer triggers a self-sustained avalanche. However, the current will continue to flow until the avalanche is quenched by the circuitry, thus temporarily lowering the electric field and restoring the device in order to be able to detect another photon. This process is complicated by the possibility that rather than being photo generated, the triggering carrier may arise from a thermal process or a trap within the multiplication region, thus leading to dark counts.

Geiger-mode operation under gated quenching has been previously demonstrated in front-illuminated GaN APDs with a single photon detection efficiency (SPDE) of 13% at a dark count rate of 400 kHz in devices with an area of 1075  $\mu\text{m}^2$ .<sup>14</sup> However, one of the major problems with GaN APDs is the rapid increase of the dark current with area and the consequent limitation of the maximum achievable gain, which has prevented the operation of larger area devices in Geiger mode. In contrast, SiC devices have shown a low dark count rate of 28 kHz for much larger 7854  $\mu\text{m}^2$  devices, but have done this with a lower SPDE of only 3.6%.<sup>15</sup>

Taking advantage of our recent work on back-illuminated GaN APDs we have already demonstrated back-illuminated GaN APDs operating in Geiger mode.<sup>16</sup> However, the realization of back-illuminated Geiger mode APDs is more complex than that of linear mode APDs due to the quenching circuitry and the need for high quality material and a very low multiplied component of the dark current. In this work, we review our recent back-illuminated GaN APDs operating in Geiger mode, and study the performance of these devices in more detail.

## 2. MATERIAL GROWTH AND DEVICE PROCESSING

### 2.1. Material Growth

The material growth and device structure are similar to those discussed earlier.<sup>17,18</sup> The material was grown in an AIXTRON 200/4-HT horizontal flow low-pressure metalorganic chemical vapor deposition (MOCVD) reactor. In order to allow for back-illumination of the device double-side polished (00.1) sapphire was used as the substrate. Growth on the sapphire substrate was nucleated with a thin 200 Å low-temperature AlN buffer layer. On top of this a 0.6- $\mu\text{m}$  thick high quality AlN template layer was grown by atomic layer epitaxy<sup>19</sup> at a temperature of  $\sim 1300^\circ\text{C}$ . This layer is transparent to wavelengths longer than 210 nm to allow back illumination of the device. Atomic force microscopy of the surface of this template show a well ordered surface with uniform atomic steps clearly visible (Figure 1: left).

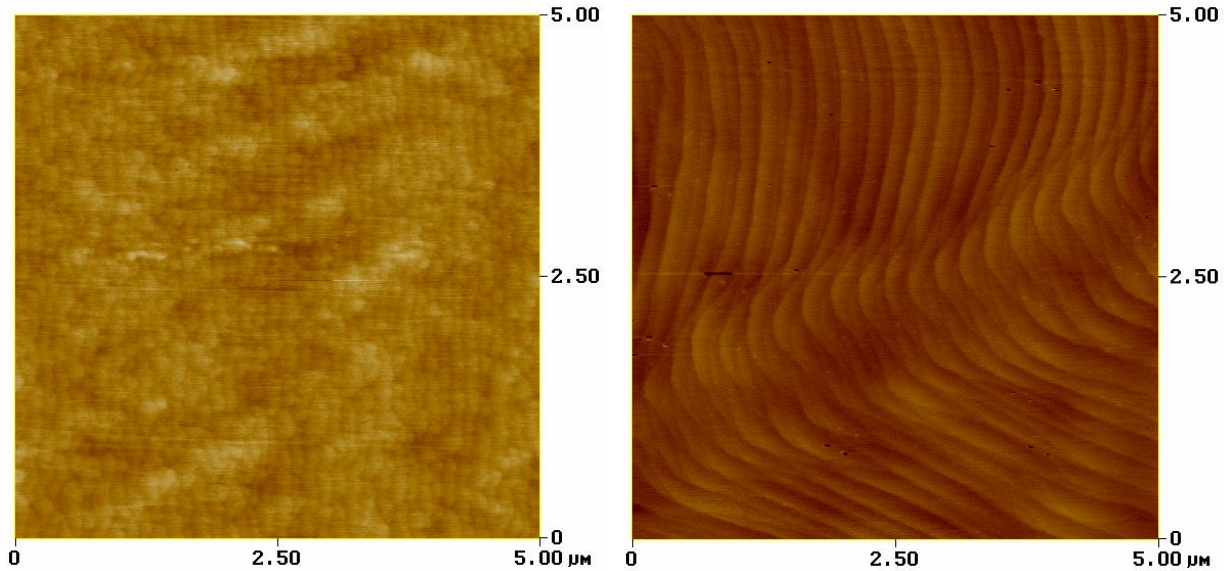
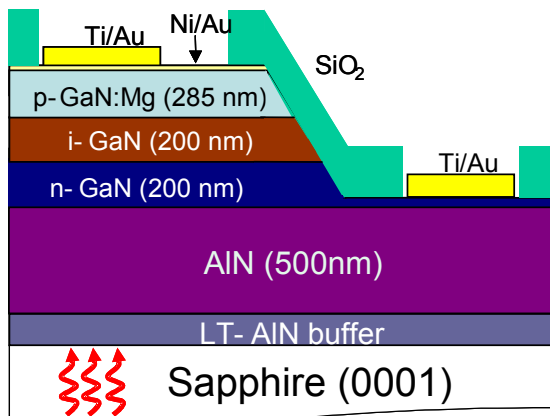


Figure 1. Left) Atomic force micrograph of the surface of a high-quality AlN template layer. Right) Atomic force micrograph of the surface of a high-quality GaN layer grown on a transparent AlN template. (vertical scale = 2.2 nm)

On top of this AlN template layer, the GaN epilayers that make up the device are grown. This is accomplished without the use of an intermediate buffer layer. The GaN layer surface is very smooth ( $\sim 1.3 \text{ \AA}$  RMS roughness) with very few observable dislocation termination pits, as shown in AFM imaging on the right of Figure 1. The active region of the device consists of a GaN *p-i-n* homojunction based structure. The p-type GaN:Mg layer has a hole concentration of  $1\text{-}3 \times 10^{18} \text{ cm}^{-3}$ , determined by Hall-effect measurements of test samples; the intrinsic GaN multiplication region has a residual concentration of  $\sim 2.5 \times 10^{16} \text{ cm}^{-3}$ , as determined by Capacitance-Voltage (C-V) measurements; and, the intentionally doped n-type GaN:Si layer has a electron concentration of  $\sim 2 \times 10^{18} \text{ cm}^{-3}$ . A schematic of the basic device structure is shown below in Figure 2.



**Back-Illuminated**

<b>Doping profile</b>	
p-GaN:Mg	( $p \sim 1\text{-}3 \times 10^{18} \text{ cm}^{-3}$ )
i-GaN	( $n \sim 1 \times 10^{16} \text{ cm}^{-3}$ )
n-GaN:Si	( $n \sim 1\text{-}2 \times 10^{18} \text{ cm}^{-3}$ )

Figure 2. The basic p-i-n Geiger mode APD structure is shown on the left, the table on the right shown the doping of the device used in the modeling and determination of the electric field profile.

## 2.2. Device Design Considerations

The interface between GaN and AlN template plays a crucial role in the performance of the device. The lattice mismatch between these two materials creates defects at the interface, which increase the recombination rate and limit the maximum EQE achievable. Hence, the thickness of the bottom *n*-GaN layer becomes critical to obtain an optimum performance. This layer separates the depletion region from the interface (Figure 3, left), so a minimum thickness is needed in order to get rid of the interface defects. However, large thicknesses reduce the EQE due to short diffusion lengths and carrier collection issues. The right of Figure 3 shows the EQE for devices with *n*-GaN thicknesses of 100, 200, and 300 nm. The optimum response is obtained for layer thicknesses of about 200 nm, which yield quantum efficiencies between 20 and 36%.

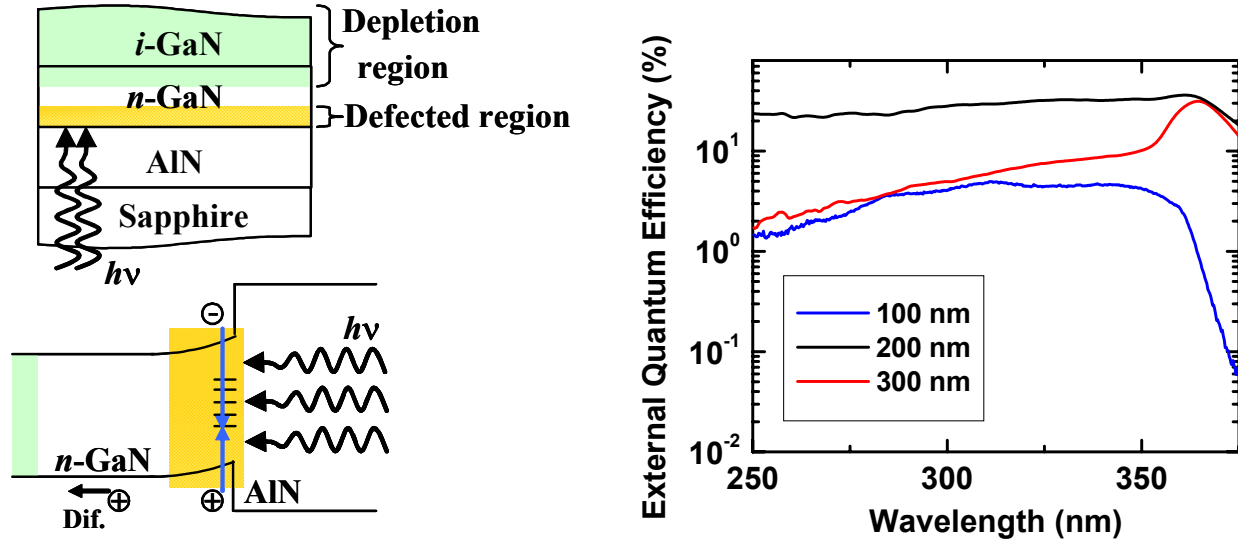


Figure 3. Left) Scheme of the device bottom layers and band diagram of the interface with the AlN template. Right) External quantum efficiency vs. wavelength for three different *n*-GaN layer thicknesses (100, 200 and 300 nm).

The thickness of the intrinsic multiplication region also plays a critical role in the performance of the device, as the multiplication is dependant on the ionization coefficients and the multiplication length. Reducing the *i*-region thickness increases the electric field for a given applied bias, thus increasing the ionization rate. However this reduces the maximum transit length the carrier can travel, and thus limits the multiplication. We have experimentally found that 200 nm to be a suitable intrinsic region thickness when coupled with a 200 nm bottom *n*-GaN layer thickness.

## 2.3. Device Processing

All samples were first rapidly thermally annealed at 1000 °C for 30 seconds under dry N<sub>2</sub> for magnesium activation in the p-type GaN:Mg layer. The material was then patterned into arrays of circular detectors with areas ranging from 225 μm<sup>2</sup> up to 14,063 μm<sup>2</sup> using electron cyclotron resonance (ECR-RF) dry etching to reach the n-type GaN:Si contact layer. A thin 30 Å Ni / 30 Å Au layer was then deposited on top of the mesas and annealed under ambient air at 500 °C for 10 minutes in order to form ohmic contact to the p-type GaN. A 400 Å Ti / 1200 Å Au metal layer was deposited on the GaN:Si layer to form the common n-type contact and on top of the thin Ni/Au as a thick metal contact to aid in contacting the device. The devices were finally covered with 300 nm of SiO<sub>2</sub> deposited by plasma enhance chemical vapor deposition to help protect the mesas and prevent premature breakdown of the devices; windows were opened via wet etching. An illustration of an array of processed diodes is shown in Figure 4 below.

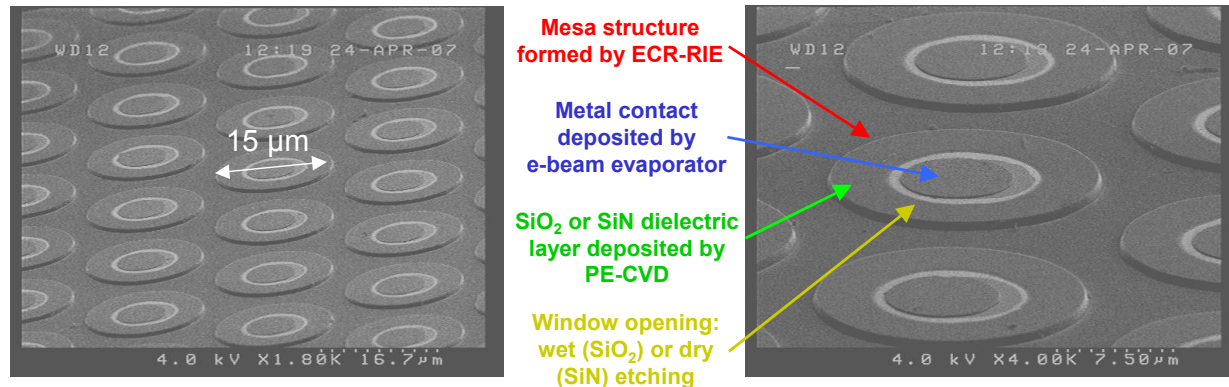


Figure 4. Scanning electron micrograph of an APD after processing. The common  $n$ -contact, not shown, is far removed from the mesas to avoid air breakdown of the devices. The arrows indicate the mesa,  $p$ -contact, passivation, and window opening.

### 3. BASIC DEVICE OPERATION

#### 3.1. Current-voltage characteristics

Prior to investigating the gain characteristics, the electrical properties of the detectors are studied at low bias. Current voltage (I-V) measurements were made in the dark using a low noise probe station and a HP 4155 semiconductor parameter analyzer. This measurement setup presents a noise floor in the 10 to 100 fA range which limits the measurement of these highly resistive devices at low biases. Under forward bias the device presents a sharp turn-on at  $\sim 3.4$  volts with a differential resistance of 8 k $\Omega$ , as shown on the left of Figure 5. Using an ideal diode model the effective series resistance and ideality factor can be extracted.<sup>17</sup> The avalanche photodiodes have an effective series resistance of 2.5 k $\Omega$ , and an ideality factor of  $\sim 2.5$ . This high series resistance is largely due to the very thin n-GaN layer necessary to allow effective back illumination of the device. This resistance will help to keep the dark current low before breakdown, but it will also serve to limit the steepness of the device break down.

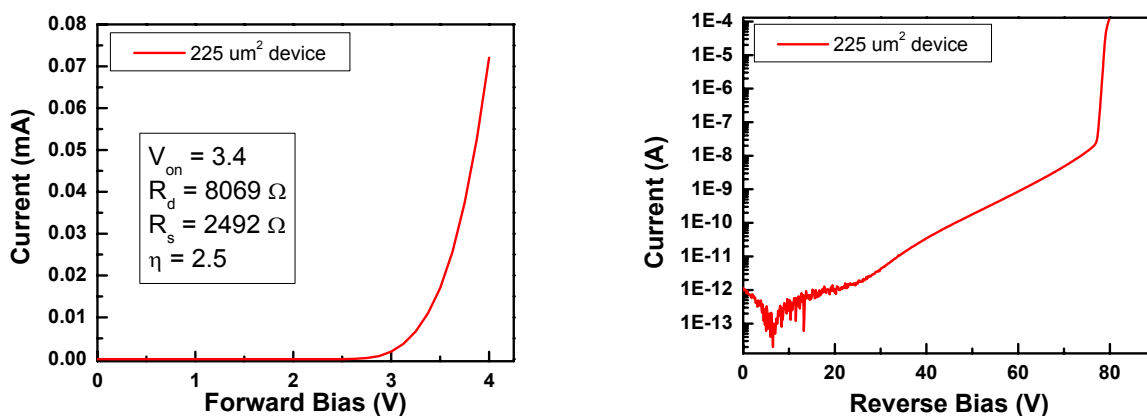


Figure 5. Left) Forward bias IV characteristic of the smallest size APDs showing the turn-on voltage, differential resistance, series resistance, and ideality factor of the diode. Right) Reverse bias IV characteristics of the diode showing a sharp breakdown at  $\sim 78$  V of reverse bias. Both curves represent the dark behavior of the diode.

Under increasing reverse bias (right of Figure 5), the device shows an exponentially increasing dark current after an initial hold-off to 35 V. This initial hold-off may be due to the initial expansion of the depletion region. As the bias is increased further the device reproducibly undergoes breakdown at a reverse bias of  $\sim 78$  V. The dark current is only  $\sim 25$  nA at the onset of breakdown; however, at breakdown, the dark current increases with a differential resistance of nearly  $70$  k $\Omega$ . When the dark current reaches into the  $100$   $\mu$ A level a saturation roll-over begins to occur, as the current is limited by the resistance of the device, compounded by internal heating effects. This process is reproducible as long as the steady state power dissipation does not exceed approximately  $50$   $\mu$ W $\cdot\mu\text{m}^{-2}$ .

### 3.2. Breakdown electric field in GaN APDs

Using a 1D finite element model<sup>20</sup>, we investigated the electric field build-up in the multiplication region. This model neglects any piezoelectric fields that may arise due to the strained GaN/AlN interface. The doping concentrations used in the model were given with the structure in Figure 2. Plots of the evolution of the modeled electric field profile are shown in Figure 6 below. From this model it is possible to estimate the electric field at the onset of gain to be  $\sim 3$  MV $\cdot\text{cm}^{-1}$

Using a simple model to consider the absorption of back-injected  $360$  nm photons in this homojunction device the relative absorption is calculated across the device, and plotted in Figure 6 below. This shows that  $88\%$  of the photons are absorbed in the  $n$ -GaN layer resulting in the injection of holes into the undoped multiplication region; however, at near breakdown, this decreases to less than  $72\%$  as the depletion region expands. The electrons generated in the multiplication region can then contribute to excess noise in linear mode APDs, however, this is less of an issue in Geiger mode APDs due to the statistical nature of the photon counting process.

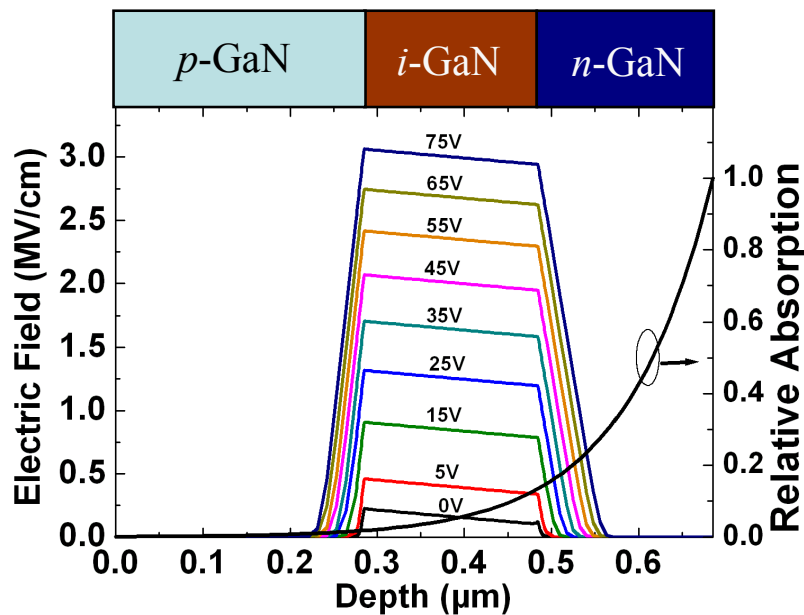


Figure 6. Electric field profile in the Geiger mode APD for various reverse biases. The relative absorption is shown on the right axis indicating most of the carriers are absorbed in the bottom  $n$ -GaN layer

### 3.3. Spectral Responsivity

A Xe lamp and a monochromator were used to illuminate the devices within the  $250$ - $450$  nm range. The light was coupled into the back of the device through an UV fiber-optic cable. The devices presented a zero-bias peak responsivity of  $\sim 80$  mA/W at  $360$  nm (Figure 7, left), with a significant decay of the response with increasing photon energy, caused by absorption in the bottom  $n$ -GaN layer. The absorption coefficient in GaN scales with the photon energy,<sup>21</sup> making shorter wavelength photons more likely to be absorbed closer to the AlN interface and thus less likely to diffuse into the depletion region.<sup>22</sup> At the onset of breakdown, a peak responsivity of  $550$  mA/W at  $360$  nm

was measured (Figure 7, right). At breakdown, the response is much flatter at short wavelengths: at these voltages, the depletion region expands almost completely to the AlN interface making detection of short wavelength photons more likely.

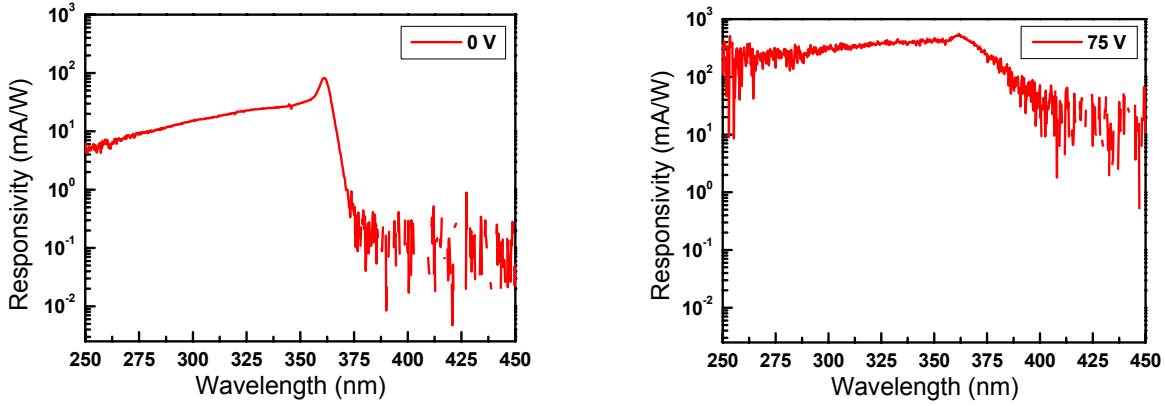


Figure 7. Left) Unbiased responsivity, Right.) Responsivity at the onset of breakdown.

The external quantum efficiency (EQE) measured at 340 nm was 9% at 0V. To determine the EQE at higher voltages, a 1D finite element model was used to estimate the photocurrent through the device as a function of bias in the absence of ionization events. This model is used to fit the experimental data at low voltages (<35 V), for which the ionization events are negligible, and then extrapolated to obtain the EQE values for higher voltages. This procedure estimates the EQE to be 29% just before breakdown. A similar fitting obtained from the analytical expression of the drift and diffusion currents corroborates this value.<sup>23</sup>

## 4. GEIGER MODE AVALANCHE OPERATION

### 4.1. Experimental setup

The same Xe-lamp and a monochromator setup was used to back-illuminate the devices via a UV fiber-optic cable. The input slit of the monochromator was adjusted to vary the photon flux, which was calibrated using a NIST traceable UV-enhanced Si detector. The APDs were measured in Geiger mode with a gated quenching circuit, as shown in Figure 8. A large reverse DC voltage ( $V_{DC}$ ) between 74 V and 78 V was applied to the APD through a 47 k $\Omega$  current limiting resistor, biasing the device just below breakdown, and a pulsed excess voltage ( $\Delta V_p$ ) between 8.5 V and 10 V was coupled in through a 50 nF capacitor to bias it above breakdown. Pulse repetition rate was 10 kHz with a pulse width of 10 ns and a dead time of 100  $\mu$ s.

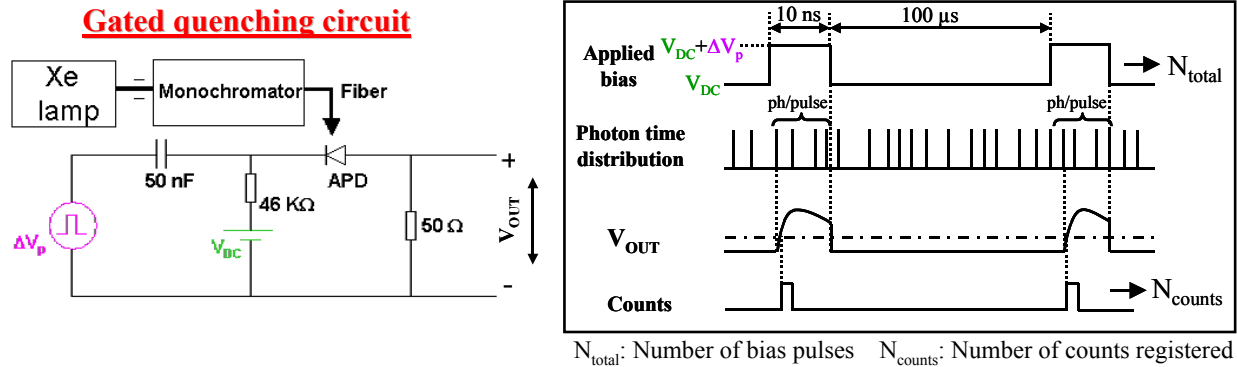


Figure 8. Left) Geiger mode APD testing circuit. Right) diagram of the applied bias, and corresponding output for a given input of photons of approximately 3 photons per pulse.

The device is then illuminated via the fiber optic, and the resulting photocurrent pulses are examined using an oscilloscope to measure the voltage drop across the 50 Ω load resistor. Alternatively, the output pulse can be fed to a Stanford Research model SR400 photon counter for threshold discrimination, and counting of the pulses. The discriminator voltage is chosen to maximize the detection efficiency while minimizing the number of spurious dark counts. The right side of Figure 8 shows a diagram of the various waveforms. This setup cannot accomplish number resolving; even if there are multiple photons per pulse, only one count will be registered. However, the devices do show a correlation between the pulse height and the number of photons per pulse (Figure 9). This could, in principle, be used to achieve photon number resolving; however there is a large tail on the distribution. The photon detection efficiency would have to be improved significantly since the effects of undetected photons are compounded when multiple photons are present in each pulse.

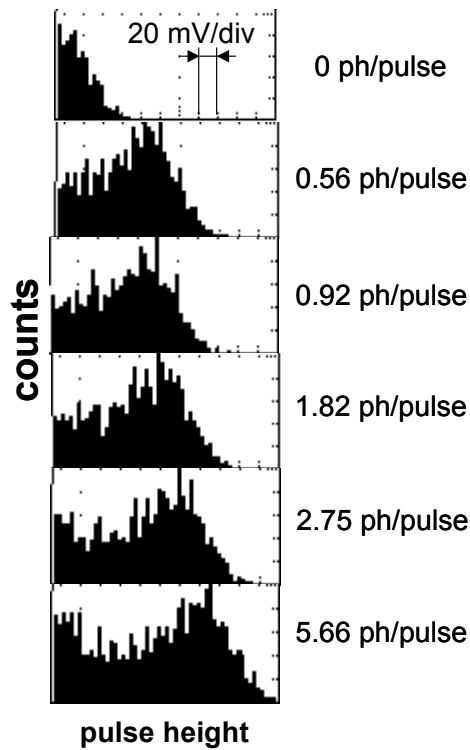


Figure 9. Histograms of pulse height for various illumination levels showing a strong variation in the maximum pulse height with the illumination level.

## 4.2. Photon Counting Operation

The detectors were illuminated with a photon flux of approximately 1 photon per pulse to determine the single photon detection efficiency (SPDE). We also attempted to measure the dark count rate (DCR) by operating the device in the dark, however for the small  $225 \mu\text{m}^2$  devices the dark count rate is below the measurement limit of 10 kHz. This low dark count rate suggests that the effect of thermal and tunneling processes on the pulse count is significantly reduced in the small area devices.<sup>24</sup> The SPDE was  $\sim 20\%$ , although a possible contribution from after-pulsing cannot be completely ruled out.

It is also worthwhile to investigate the pulse detection efficiency as a function of the photon flux in order to identify the minimum photon flux for effective operation, i.e. the minimum photon flux necessary to ensure a pulse detection efficiency of 100%. Figure 10 shows the pulse detection efficiency as a function of illumination. The photon flux needs to be at least 3 photons per pulse to ensure having a 100% probability of registering a least one count per pulse

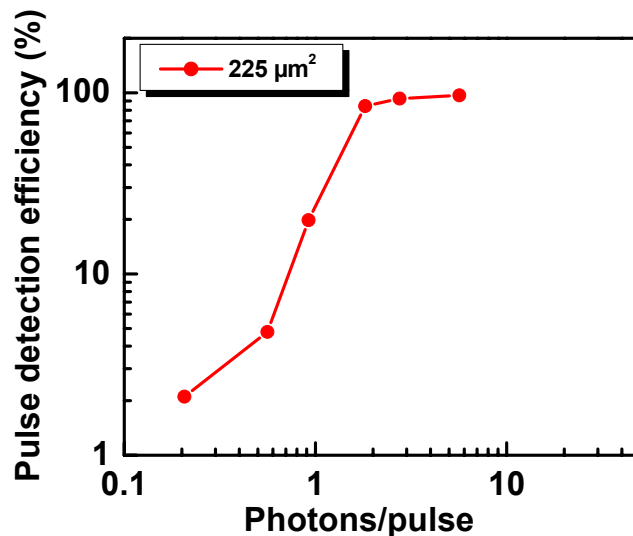


Figure 10. Pulse detection efficiency as a function of illumination (in photons per pulse) for a  $225 \mu\text{m}^2$  Geiger mode APD showing a minimum photon flux for effective operation of  $\sim 3$  photons per pulse.

## 4.3. Spectral Response

In order to investigate the spectral response in photon counting mode and the uniformity of that response, four different devices were scanned from 230 nm to 400 nm with a photon flux of about 1 photon per pulse. The average SPDE as a function of wavelength is shown with error bars in Figure 11. Reasonably flat detection efficiency was obtained for photon energies above the bandgap; below the bandgap, a sharp cut-off and a high visible light rejection ratio are observed.

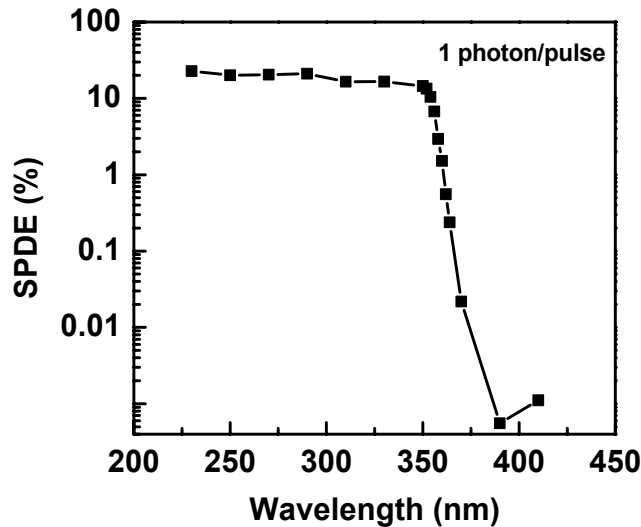


Figure 11. Photon counting spectral response of a device obtained at a  $V_{DC}$  of 77V and a  $\Delta V_p$  of 10 V.

## 5. CONCLUSION

In summary, back-illuminated GaN APDs operating in Geiger-mode capable of single photon counting have been presented and studied. These devices show a SPDEs of 20% and dark count rates <10KHz. The spectral response shows a flat Geiger-mode response for photon energies above the bandgap, and a high visible-light rejection ratio.

## ACKNOWLEDGEMENTS

J.L. Pau acknowledges the support of the Fulbright Association and the Spanish Ministry of Education and Science. The authors would like to acknowledge Dr. Donald Silversmith (AFOSR), and Dr. Henryk Temkin (DARPA) for their support and encouragement.

## REFERENCES

1. P. Kung, A Yasan, R. McClintock, S.R. Darvish, K. Mi, M. Razeghi, "Future of AlxGa1-xN materials and device technology for ultraviolet photodetectors", Proc. SPIE, vol. **4650**, pp.199-206, (2002).
2. M. Razeghi, "Short-wavelength solar-blind detectors- status, prospects, and markets", Proc. IEEE, vol. **90**, pp. 1006-1014, (2002).
3. M. Ulmer, M. Razeghi, E. Bigan, "Ultra-Violet Detectors for Astrophysics, Present and Future," Proc. SPIE vol. **2397** pp. 210-216, (1995).
4. Hamamatsu Photonics, K.K., <http://usa.hamamatsu.com/>, PMTs based upon Cs-Te photocathodes such as R1080.
5. DARPA BAA06-14, Deep Ultraviolet Avalanche Photodetectors (DUVAP), (2005)
6. J. L. Pau, E. Monroy, M. A. Sánchez-García, E. Calleja, and E. Munoz, "AlGaIn ultraviolet photodetectors grown by molecular beam epitaxy on Si(111) substrates", Materials Science and Engineering B **93**, 159 (2002).
7. K. McIntosh, R. Molnar, L. Mahoney, M. Geis, K. Molvar, I. Melngailis, R. Aggarwal, W. Goodhue, S. Choi, and D. Spears, "GaN avalanche photodiodes grown by hydride vapor-phase epitaxy", Appl. Phys. Lett. **75**, 3485 (1999).
8. J. Carrano, D. Lambert, C. Eiting, C. Collins, T. Li, S. Wang, A. Beck, R. Dupuis, and J. Campbell, "GaN avalanche photodiodes", Appl. Phys. Lett. **76**, 924 (2000).
9. B. Yang, T. Li, K. Heng, C. Collins, S. Wang, J. Carrano, R. Dupuis, J. Campbell, M. Schurman, and I. Ferguson, "Low dark current GaN avalanche photodiodes", IEEE J. Quantum Electron. **36**, 1389 (2000).

- 
10. S. Verghese, K. McIntosh, R. Molnar, L. Mahoney, R. Aggarwal, M. Geis, K. Molvar, E. Duerr, and I. Melngailis, "GaN avalanche photodiodes operating in linear-gain mode and Geiger mode", *IEEE Trans. Elect. Dev.* **48**, 502 (2001).
  11. J.B. Limb, D. Yoo, J.H. Ryou, W. Lee, S.C. Shen, R.D. Dupuis, M.L. Reed, C.J. Collins, M. Wraback, D. Hanser, E. Preble, N.M. Williams, and K. Evans, "GaN ultraviolet avalanche photodiodes with optical gain greater than 1000 grown on GaN substrates by metal-organic chemical vapor deposition", *Appl. Phys. Lett.* **89**, 11112 (2006).
  12. I.J. Oguzman, E. Bellotti, K. Brennan, J. Kolnik, R. Wang, and P. Ruden, "Theory of hole initiated impact ionization in bulk zincblende and wurtzite GaN", *J. Appl. Phys.* **81**, 7827 (1997).
  13. R. McClintock, J. L. Pau, K. Minder, C. Bayram, P. Kung, M. Razeghi, *Appl. Phys. Lett.* **90**, 1411121 (2007).
  14. K. A. McIntosh, R. J. Molnar, L. J. Mahoney, K. M. Molvar, N. Efremow, Jr., S. Verghese, *Appl. Phys. Lett.* **76**, 3938 (2000).
  15. A. L. Beck, X. Guo, H.-D. Liu, A. Ghatak-roy, J. C. Campbell, *Proc. SPIE* **6372**, 637200-1(2006).
  16. J. L. Pau, R. McClintock, K. Minder, C. Bayram, P. Kung, M. Razeghi, E. Muñoz, and D. Silversmith, "Geiger-mode operation of back-illuminated GaN avalanche photodiodes", *Applied Physics Letters* **91**(4), 041104 -1 (2007).
  17. R. McClintock, A. Yasan, K. Mayes, D. Shiell, S.R. Darvish, P. Kung, and M. Razeghi, "High Quantum Efficiency Solar-Blind Photodetectors", *Proc. SPIE* **5359**, 434 (2004).
  18. P. Kung, R. McClintock, J. Pau Vizcaino, K. Minder, C. Bayram and M. Razeghi, "III-Nitride Avalanche Photodiodes", *Proc. SPIE* **6479**, 64791J-1-12 (2007)
  19. J. Zhang, H. Wang, W. Sun, V. Adivarahan, S. Wu, A. Chitnis, C. Chen, M. Shatalov, E. Kuokstis, J. Yang, and M. Asif Khan, "High-quality AlGaIn layers over pulsed atomic-layer epitaxially grown AlN templates for deep ultraviolet light-emitting diodes", *J. Elect. Mat.* **32**, 364 (2003).
  20. D. Winston and R. Hayes, "SimWindows - A New Simulator for Studying Quantum-well Optoelectronic Devices" *Compound Semiconductors 1994 Institute of Physics Conference Series* **141**, 747 (1995).
  21. J. F. Muth, J. D. Brown, M. A. L. Johnson, Z. Yu, R. M. Kolbas, J. W. Cook, Jr., and J. F. Schetzina, *MRS Internet J. of Nitride Semicond. Res.*, **4S1**, 1 (1999).
  22. E. Monroy, F. Calle, J. L. Pau, F. J. Sanchez, E. Munoz, F. Omnes, B. Beaumont, and P. Gibart, *Journal of Applied Physics* **88**, 2081 (2000).
  23. S. M. Sze, *Physics of Semiconductor Devices* (Wiley, New York 1981), Chap. 13, p. 754.
  24. K. E. Jensen, P. I. Hopman, E. K. Duerr, E. A. Dauler, J. P. Donnelly, S. H. Groves, L. J. Mahoney, K. A. McIntosh, K. M. Molvar, A. Napoleone, D. C. Oakley, S. Verghese, C. J. Vineis, R. D. Younger, *Appl. Phys. Lett.* **88**, 133503 (2006).